6

Dysprosium Doped $LiMn_{2-x}Dy_xO_4$ (0x=0.01, 0.02, 0.03, 0.04, 0.05) Cathodes

The chapter is composed of four sections and eight sub-sections. The section 6.1 provides introduction and need of varied amount dysprosium doped $LiMn_2O_4$ (LMO) cathode materials. The physical characterizations of dysprosium doped LMO cathode powders are presented in section 6.2. The section 6.3 is offering the out comes from electrochemical characterization of cathode materials. The section 6.2 and 6.3 are further divided into subsections. The section 6.2 is partitioned in four sub-sections namely: the sub-section 6.2.1 describes the crystal structural parameters; the sub-section 6.2.2 presents the surface morphology and elemental information, the sub-section 6.2.3 states the thermo-gravimetric performance. The section 6.3 is also sorted in four sub-sections which include cyclic voltammetry study in sub-section 6.3.1, the galvanostatic charge-discharge performance in sub-section 6.3.2, the rate performance and Cyclability analysis in sub-section 6.3.3 and electrochemical impedance spectroscopy in sub-section 6.3.4. At the end of the chapter, the concluding remarks are given in section 6.4.

6.1 INTRODUCTION

The dysprosium doped spinel cathode, $LiMn_{2-x}Dy_xO_4$ (x=0.0, 0.05, 0.1, 0.15, and 0.02), was synthesized via double stage co-precipitation method and microwave heat treatment [Balaji et al, 2012]. The different rare-earth (RE) elemental doped, $LiMn_{2-x}RE_xO_4$ (RE = Gd, Tb, Dy and Yb; x=0.05), spinel cathodes were studied in Chapter 4. The results showed that the doping of gadolinium (Gd) and dysprosium (Dy) elements offer better performance compared to undoped LMO and other RE, terbium (Tb) and ytterbium (Yb), elements. The study about the optimization of doping amount in case of gadolinium element has discussed in Chapter 4. The findings supported that the $LiMn_{1.96}Gd_{0.04}O_4$ (LMO-Gd04) cathode was performing better in comparison to other cathode materials as LMO, $LiMn_{1.96}Gd_{0.02}O_4$ (LMO-Gd02) and $LiMn_{1.96}Gd_{0.05}O_4$ (LMO-Gd05). The current chapter is devoted to the dysprosium elemental doping effects on spinel structure cathode which delivers improved battery performance. The coding of synthesized cathodes is done as $LiMn_2O_4$ (LMO), $LiMn_{1.99}Dy_{0.01}O_4$ (LMO-Dy01), $LiMn_{1.98}Dy_{0.02}O_4$ (LMO-Dy02), $LiMn_{1.97}Dy_{0.03}O_4$ (LMO-Dy03), $LiMn_{1.96}Dy_{0.04}O_4$ (LMO-Dy04) and $LiMn_{1.95}Dy_{0.05}O_4$ (LMO-Dy05). The code name of Dy doped cathodes are tabulated in Table 2.1 and used here after.

The spinel phase LMO cathode material and its dysprosium doped derivatives, $LiMn_{2-x}Dy_xO_4$ (x=0, 0.01, 0.02, 0.04, 0.05), are prepared using the organic sol-gel method as discussed in sub-section 3.2.2 in Chapter 3. The cathode samples are characterized and analyzed to investigate the effect of varied amount of dysprosium doping on physical and electrochemical performance. The purpose of the study is to optimize the dysprosium doping concentration.

6.2 PHYSICAL CHARACTERIZATION OF DYSPROSIUM DOPED $LiMn_2O_4$ CATHODES

The as synthesized dysprosium doped cathode, $LiMn_{2-x}Dy_xO_4$ (x=0, 0.01, 0.02, 0.03, 0.04, and 0.05), materials are characterized to assess the physical effects on cathode materials. The thermal stability of synthesized cathode materials is not assessed for $LiMn_{1.99}Dy_{0.01}O_4$ (LMO-Dy01), $LiMn_{1.98}Dy_{0.02}O_4$ (LMO-Dy02), $LiMn_{1.97}Dy_{0.03}O_4$ (LMO-Dy03), and $LiMn_{1.96}Dy_{0.04}O_4$ (LMO-Dy04). The findings about TGA study, in sub section 4.2.3 in Chapter 4, supported that the $LiMn_{1.95}Dy_{0.05}O_4$ (LMO-Dy05) was more thermally stable compared to LMO and LMO-Gd05. And also, the synthesis of dysprosium doped cathode materials is adopted here

by same procedure. The battery characterizations are presented in subsequent sub-sections from 6.2.1 to 6.2.4 as following:

(6.2.1) *X-ray diffraction pattern and analysis* are delivering information about spinel phase purity and lattice parameters.
(6.2.2) *Surface morphology and analysis* are expressing the powder's surface morphology, geometrical shape and size.
(6.2.3) *Energy dispersive x-ray (EDX) spectra and analysis* are providing insight about the elemental detection and their stoichiometric ratio.
(6.2.4) *Brunauer-Emmett-Teller (BET) and analysis* are describing specific surface area and porosity of cathodes powder

6.2.1 X-ray Diffraction and Structure Analysis

The spinel phase information in all as synthesized powders of undoped LMO and Dy doped derivatives, $LiMn_{2-x}Dy_xO_4$ (x=0, 0.01, 0.02, 0.03, 0.04, 0.05), are obtained by recording x-ray diffraction patterns. The recorded x-ray diffraction pattern of as synthesized cathode powders calcined at 800 ^{O}C for 14 h are shown in Figure 6.1. The two theta angle was scanned from 10° to 80° angle with fixed scan rate at ~ 1° per minute. The x-ray-diffraction principle has discussed in sub-section 3.3.1 of Chapter 3. The cubic spinel phase, $Fd\bar{3}m$ (space group: 227), characteristic peaks are observed and matched with JCPDS file (35-0782) [Hung et al, 2007]. These peaks are observed at 18.66°, 36.12°, 37.78°, 43.90°, 48.08°, 58.12°, 63.82°, and 67.14° two theta angles and assigned to plane (111), (311), (222), (400), (311), (511), (440), and (531), respectively. Among these peaks, the peak at two theta angle 18.66°, corresponds to plan (111), is having highest intensity in all cathodes. The cubic spinel phase purity is obtained by Reitveld method. The purity of cubic spinel phase is as 100 %, 77.72 %, 88.16 %, 88.76 %, 90.67 % and 90.86 % for LMO, LMO-Dy01, LMO-Dy02, LMO-Dy03, LMO-Dy04 and LMO-Dy05 cathode powders respectively. The impure phases are Mn_2O_3 and $DyMn_2O_5$ phases. As Dy doping amount increased, the $DyMn_2O_5$ phase is also increased from 1.67% to 7.35% whereas the phase Mn_2O_3 is fluctuating and varied from 1.80 - 9.35 %. These impure phase formation is initiated at high temperature (800 °C) which are initial condition for their formation. However, percentage contribution of these phases is less. The similar results are reported in literature in case of Dy[Balaji et al, 2012], Sm [Balaji et al, 2010], Tb [Lee et al, 2012], and Gd [Han et al, 2012]. The lattice parameters such as lattice constant, volume of unit cell, crystalline size are calculated using the Retieveld method and tabulated in Table 6.1. The full width at half maxima (FWHM) corresponds to plan (111) is calculated directly from diffraction pattern. The integral peak intensity ratio [$I_{(400)}/I_{(311)}$] are calculated using integral area of peak module.

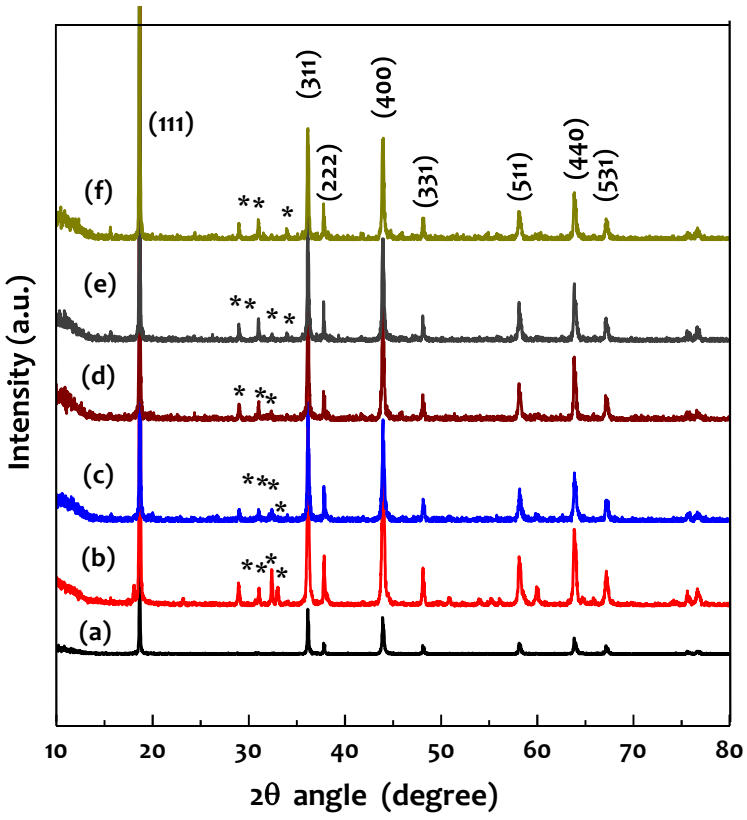

Figure 6.1: XRD pattern of (a) $LiMn_2O_4$, (b) $LiMn_{1.99}Dy_{0.01}O_4$, (c) $LiMn_{1.98}Dy_{0.02}O_4$, (d) $LiMn_{1.97}Dy_{0.03}O_4$, (e) $LiMn_{1.96}Dy_{0.04}O_4$ and (f) $LiMn_{1.5}Dy_{0.05}O_4$ powders calcined at 800 ˚C /14 h

The lattice constant for LMO is observed 8.24304Å which was similar to reported in literature [Balaji et al, 2012]. The lattice constants are observed as 8.24501 Å, 8.24401 Å, 8.24307 Å, 8.24275 Å, and 8.24163 Å for Dy doped cathodes LMO-Dy01, LMO-Dy02, LMO-Dy03, LMO-Dy04 and LMO-Dy05, respectively. The lattice constant is reduced as Dy doping amount increased. The similar reports are available in literature [Balaji et al, 2012]. The integral intensity ratio of planes (I_{400}/I_{311}) for Dy doped cathode is providing insight about the substitution of dopant Dy^{3+} ion at octahedral site in place of the manganese ,Mn^{3+}, ion [Ohzuku et al, 2001; Balaji et al, 2012]. The results showed that the integral intensity ratio is decreased as Dy doping amount increased which is evidence for more Dy^{3+} substitutions. The similar behavior was observed in Dy doped cathode study outcomes [Balaji et al, 2012].

Table 6.1: Lattice Structure Parameter for $LiMn_2O_4$ and $LiMn_{2-x}Dy_xO_4$ (x = 0.01, 0.02, 0.03, 0.04, 0.05) Powders

Sample Description	*Lattice Constant*	*Unit Cell Volume*	*FWHM*	*Crystallite Size*	*Cubic Spinel Phase*	$I_{(400)}/I_{(311)}$
	(Å)	($Å^3$)	(°)	(Å)	(%)	
LMO	8.24304	560.095	0.100	206.6	100	1.062
LMO-Dy01	8.24501	560.498	0.131	111.0	77.719	1.060
LMO-Dy02	8.24401	560.292	0.118	122.4	88.158	1.051
LMO-Dy03	8.24307	560.102	0.114	125.9	88.761	1.030
LMO-Dy04	8.24275	560.036	0.101	140.9	90.673	1.014
LMO-Dy05	8.24163	559.821	0.105	180.6	90.857	1.011

6.2.2 Surface Morphology and Its Analysis

The as synthesized cathode powders are studied to visualize the surface morphology through scanning electron microscopy (SEM). The images of surface morphology for $LiMn_{2-x}Dy_xO_4$ (x=0, 0.01, 0.02, 0.03, 0.04, 0.05) spinel cathodes are recorded at 10.0 KX by applying EHT 20.0 KV and current 80-100 pA on electron gun. The sample preparation is discussed in sub-section 3.3.2 of Chapter 3. The obtained graphics are shown in Figure 6.2 (a-f). One may note that the particles size is non-uniform and polyhedral in shape. The particle size is varied from 1 µm to 600 nm. The agglomeration in particles is evidently seen. The tendency of large particle formation is reduced with increase Dy doping amount as can be seen from Figure 6.2 (a-f).

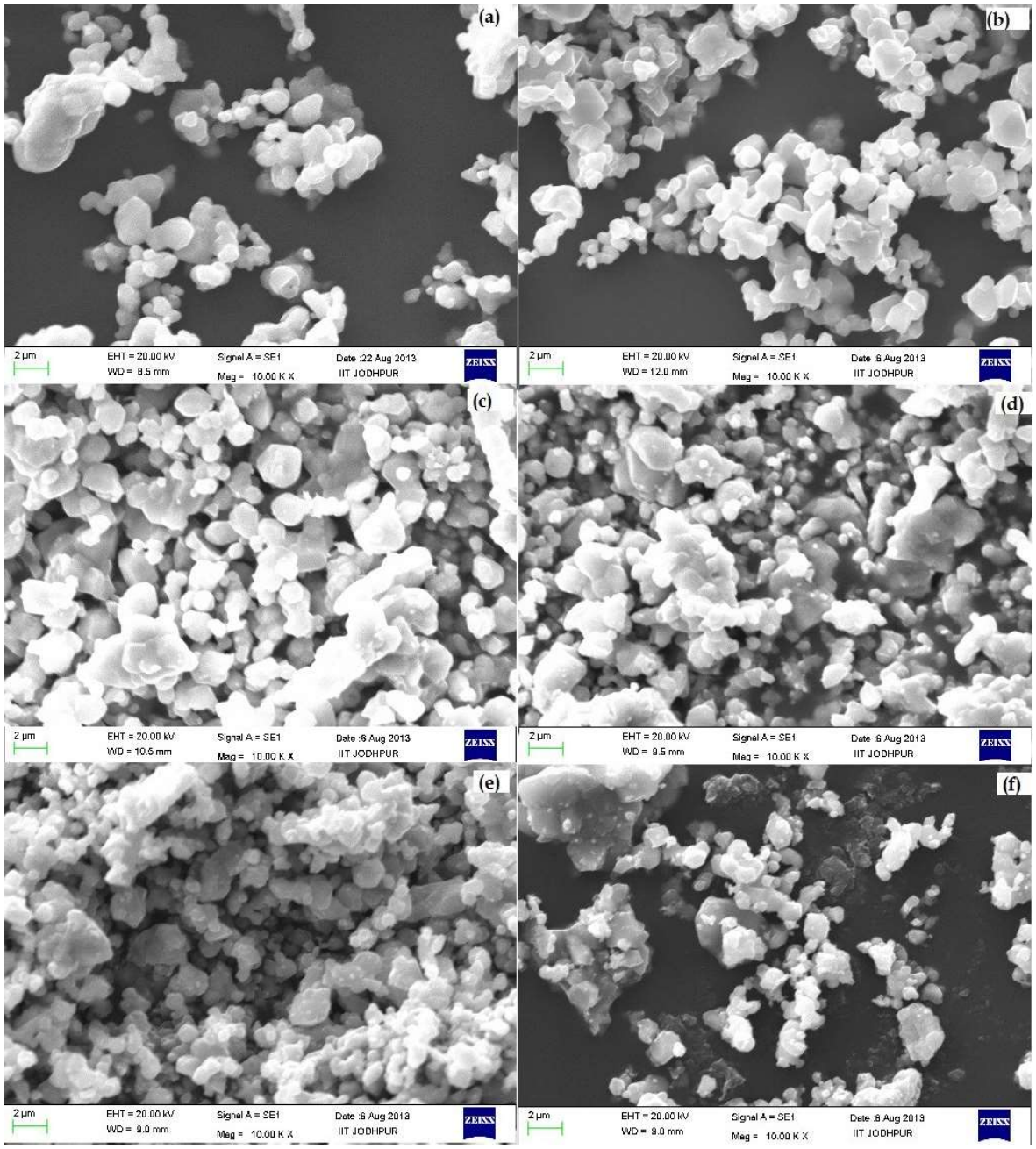

Figure 6.2: Scanning electron microscope image of (a) $LiMn_2O_4$, (b) $LiMn_{1.99}Dy_{0.01}O_4$, (c) $LiMn_{1.98}Dy_{0.02}O_4$, (d) $LiMn_{1.97}Dy_{0.03}O_4$, (e) $LiMn_{1.96}Dy_{0.04}O_4$ and (f) $LiMn_{1.5}Dy_{0.05}O_4$ powders calcined at 800 °C / 14 h

The particles size and surface morphology play a vital role in Li-ion diffusion and formation of slid electrolyte interface (SEI) during the charging and discharging process of fabricated coin/ Swagelok cell. The uniform particle size and regular geometry enable smooth Li-ion diffusion and reduction in SEI width which have direct impact on reversibility and recyclability of cell.

6.2.3 Energy Dispersive X-ray Spectra and Its Analysis

The elemental existence in as synthesized cubic spinel phase cathode materials, $LiMn_{2-x}Dy_xO_4$ (x=0, 0.01, 0.02, 0.03, 0.04, 0.05), are investigated through EDX assembly attached with SEM EVO.

Table 6.2: Elemental Composition of $LiMn_2O_4$ and $LiMn_{2-x}Dy_xO_4$ (x = 0.01, 0.02, 0.03, 0.04, 0.05) Powders

Sample Description	*Observed Atomic (%)*			*Theoretical Atomic (%)*		
	Mn	*O*	*Dy*	*Mn*	*O*	*Dy*
LMO	33.71	66.29	0.0	33.33	66.66	0.0
LMO-Dy01	34.51	65.27	0.22	33.17	66.67	0.17
LMO-Dy02	31.92	67.66	0.42	33.00	66.67	0.33
LMO-Dy03	33.01	66.34	0.57	32.83	66.67	0.50
LMO-Dy04	31.99	67.34	0.67	32.67	66.67	0.67
LMO-Dy05	32.77	66.43	0.80	32.5	66.66	0.83

The synthesized active materials are in pure elemental form. It is confirmed by the absence of other elements in the EDX spectrum as shown in Figure 6.3. The electron beam current is adjusted at ~ 1-2 nm. The elemental compositions in terms of atomic percentage as reported by the EDX are tabulated in Table 6.2. It is compared with theoretical composition of atomic percentage. The theoretical and experimental observations are not in equal proportionate. It is deviating little from atomic stoichiometric ratio.

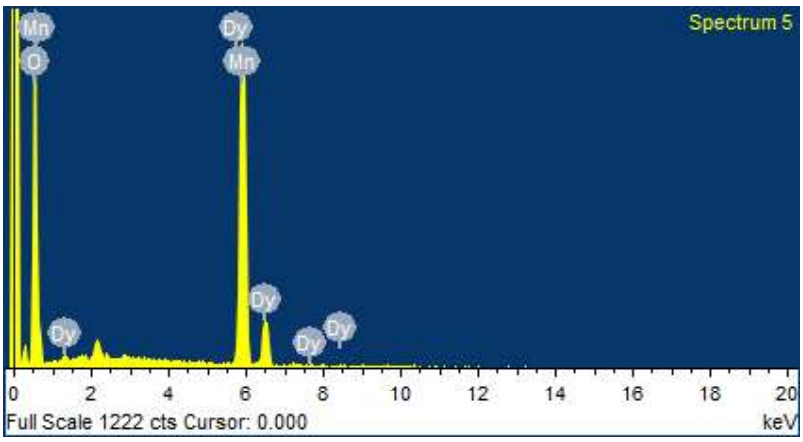

Figure 6.3: EDX spectrum for $LiMn_{2-x}Dy_xO_4$ (x = 0, 0.01, 0.02, 0.03, 0.04, 0.05) powders calcined at 800 ˚C / 14 h

6.2.4 Porosity and Specific Surface Area Analysis

The nitrogen adsorption-desorption isotherms and pore size distributions are shown in Figure 6.4 (a-b). The specific surface areas are measured as 1.0-2.5 m^2/g by multi point Brunauer-Emmett-Teller (BET) method for LMO-Dy02, LMO-Dy03, LMO-Dy04, and LMO-Dy05 cathodes and shown in Figure 6.4 (a). The specific surface area for LMO-Dy03 is measured as 2.5 m^2/g whereas for LMO-Dy04 is observed as 1.0 m^2/g. The pore-size distribution, Figure 6.4 (b), reveals that the different materials show a narrow range of pore sizes from 2 to 5 nm,

with an average pore size of 3 nm. Thus, synthesized cathode samples have a more homogeneous and uniform surface morphology.

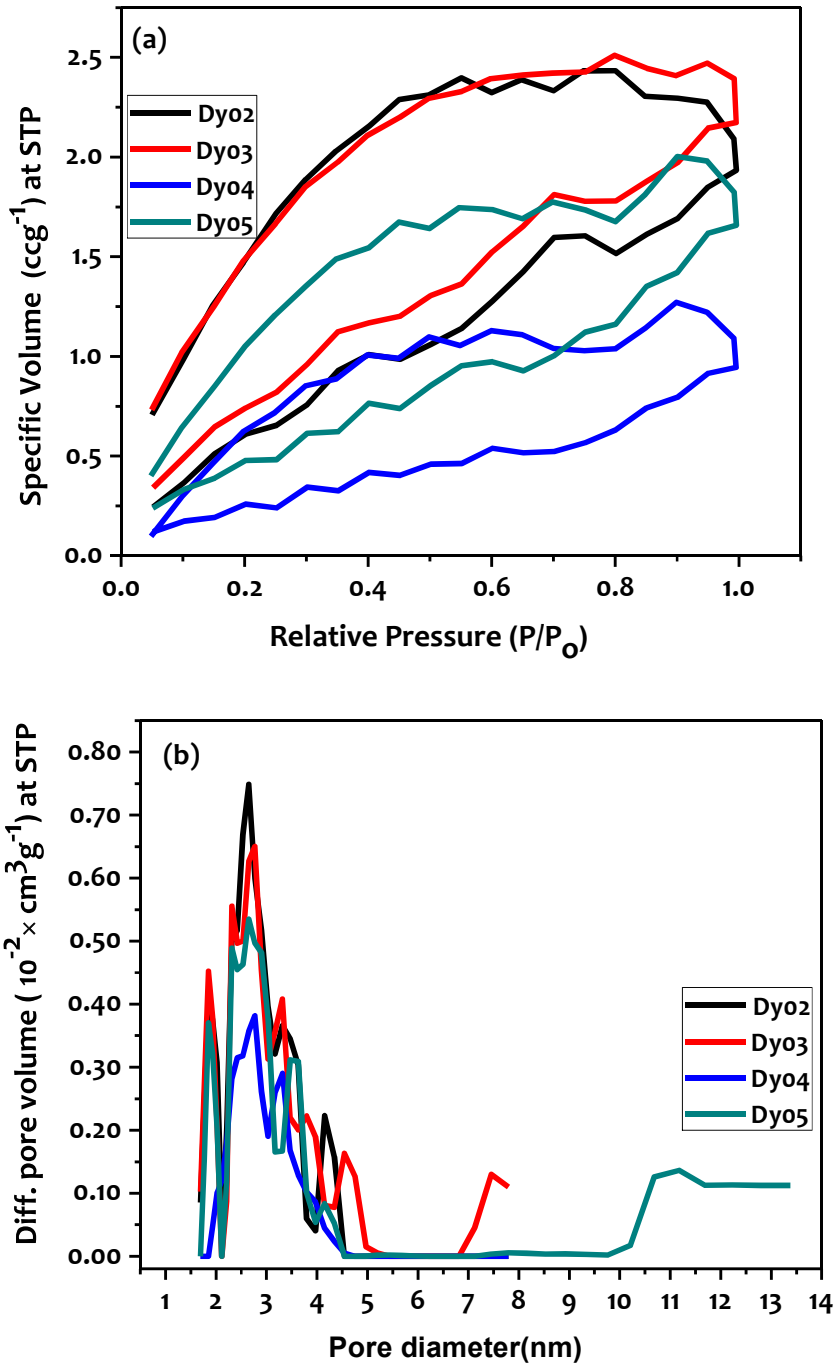

Figure 6.4: (a) Nitrogen adsorption - desorption isotherms and (b) Pore size distribution for $LiMn_{2-x}Dy_xO_4$, (x=0.02, 0.03, 0.04, 0.05) powders

6.3 ELECTROCHEMICAL CHARACTERIZATION OF DYSPROSIUM DOPED $LiMn_2O_4$ CATHODES

The as synthesized rare-earth dysprosium element doped, $LiMn_{2-x}Dy_xO_4$ (x=0, 0.01, 0.02, 0.03, 0.04, and 0.05), powders are characterized by electrochemically to evaluate the influence of different amount of Dy doping on battery parameter performance. The electrochemical performances of active material are assessed by adopting cyclic voltammetry technique,

galvanostatic charge-discharge technique, and AC impedance spectroscopy technique. The obtained results from these characterization techniques are presented in subsequent sub-sections from 6.3.1 to 6.3.4 for more insight:

(6.3.1) *Cyclic voltammetry technique:* It is exploring redox potentials of synthesized Dy doped cathode material with respect to Li/Li^+.

(6.3.2) *Galvanostatic charge-discharge technique*: It is evaluating specific charge-discharge capacities at different charge and discharge rates i.e. C-rate.

(6.3.3) *Rate performance:* It is presenting the capacity at different C-rates.

(6.3.4) *AC impedance spectroscopy:* It is measuring the total internal resistance of fabricated Swagelok cell.

To analyze the electrochemical properties of as synthesized cathode materials, the fabrication of cathodes and assembling of swagelok cell are carried out as discussed in sub-section 3.41.4 of Chapter 3. The cathodes are prepared using 80% active material, 10% carbon black and 10% PVDF. The two/three electrode swaglok cells are assembled in inert gas ,Ar –gas, atmosphere with $H_2O < 1$ PPM and $O_2 < 4$ PPM.

6.3.1 Cyclic Voltammetry and Its Analysis

The fabricated 8.0 mm diameter cathodes of LMO and $LiMn_{2-x}Dy_xO_4$ (x= 0.01, 0.02, 0.03, 0.04, 0.05) are used to assemble the three electrode swagelok cell for cyclic voltammetry (CV) study. The Swagelok cell electrodes are as working electrode (as cathode of LMO and $LiMn_{2-x}Dy_xO_4$), counter electrode (as anode of Li metal foil) and reference electrode (as Li metal foil). The cyclic voltammetry is performed within potential 3.5 - 4.5 V with scan rate 0.1 mV/sec. The CV curves are presented in Figure 6.5. The reduction and oxidation potential of active material are assessed with reference to Li/Li^+-ion.

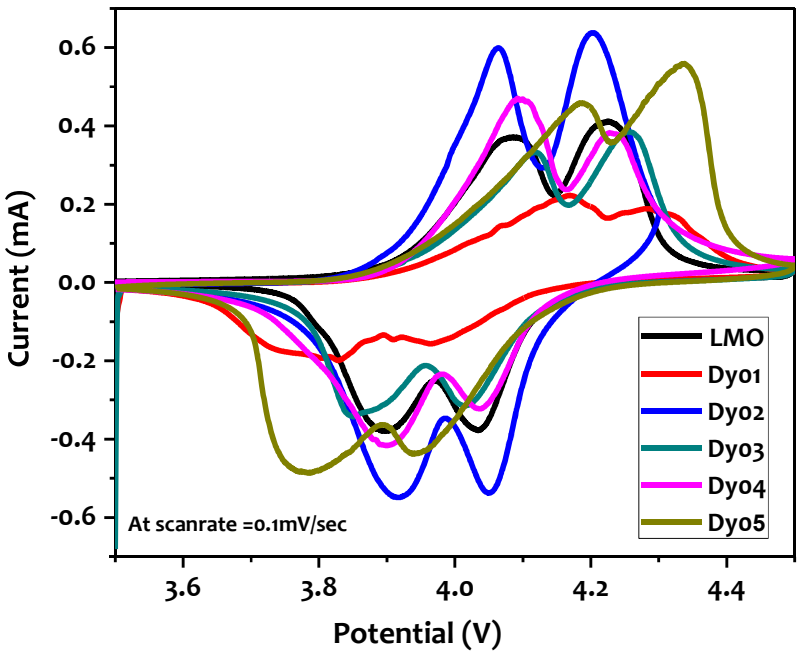

Figure 6.5: Cyclic voltammetry of $LiMn_2O_4$ and $LiMn_{2-x}Dy_xO_4$ (x= 0.01, 0.02, 0.03, 0.04, 0.05) cathodes

The two redox peaks in all cathode materials are indicating two stages intercalation/de-intercalation process. The oxidation and reduction peaks are obtained at 4.08 V, 4.22 V and 3.89 V, 4.03 V respectively in the case of spinel LMO cathode. The oxidation and reduction peaks for Dy doped derivatives are also observed nearby LMO cathode and tabulated in Table 6.3. The

lower difference in anodic potential in LMO-Dy02 cathode is showing less polarization potential compared to other cathodes. It is supported by the high current which is observed during oxidation and reduction steps as shown in Figure 6.5.

Table 6.3: Redox Potential of $LiMn_2O_4$ and $LiMn_{2-x}Dy_xO_4$ (x = 0.01, 0.02, 0.03, 0.04, 0.05) Cathodes

Sample Description	*Potential (V)*					
	E_{pa1}	E_{pa2}	E_{pc1}	E_{pc2}	ΔE_{p1}	ΔE_{p2}
LMO	4.08	4.22	3.89	4.03	0.19	0.33
LMO-Dy01	4.16	4.29	3.82	3.96	0.34	0.33
LMO-Dy02	4.06	4.20	3.91	4.05	0.15	0.15
LMO-Dy03	4.11	4.25	3.84	4.01	0.27	0.24
LMO-Dy04	4.09	4.23	3.89	4.03	0.20	0.20
LMO-Dy05	4.18	4.33	3.77	3.94	0.41	0.39

6.3.2 Galvanostatic Charge-Discharge Performance and Its Analysis

The galvanostatic charge-discharge studies are performed for LMO and $LiMn_{2-x}Dy_xO_4$ (x= 0.01, 0.02, 0.03, 0.04, 0.05) cathode materials at C/10, C/5 and C/10 (recv.) rate. The specific charge-discharge capacities are measured and tabulated in Table (6.4-6.6). The initial charge-discharge capacities at C/10 and C/5 for LMO and $LiMn_{2-x}Dy_xO_4$ (x= 0.01, 0.02, 0.03, 0.04, 0.05) cathode materials are presented in Figure6.6. The initial specific charge and discharge capacities at C/10 rate are observed as 121.7, 158. 7, 154.0, 100.7, 108.1, 103.4 and 118.1, 124.1, 124.7, 81.9, 93.3, 95.5 $mAhg^{-1}$ for $LiMn_{2-x}Dy_xO_4$ (x= 0, 0.01, 0.02, 0.03, 0.04, and 0.05) cathode materials, respectively. The columbic efficiency in initial charge – discharge cycle is observed as 97.52%, 78.48%, 80.51%, 81.33%, 86.21% and 92.51% for all these cathode materials. The percentage of capacity fading after 10 cycles at C/10 are 35.26%, 38.65%, 33.76%, 22.10%, 22.85%, and 25.96% for $LiMn_{2-x}Dy_xO_4$ (x = 0, 0.01, 0.02, 0.03, 0.04, and 0.05) cathodes respectively.

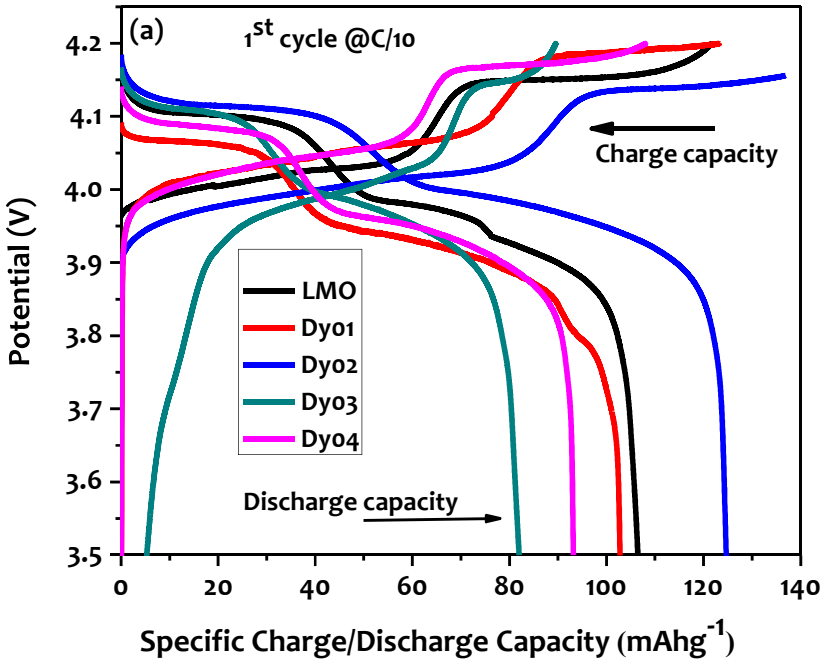

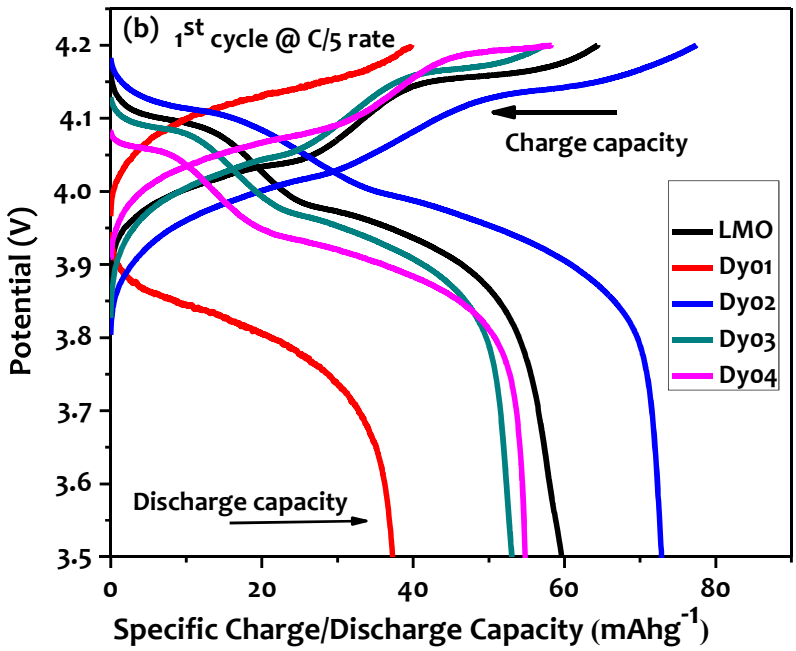

Figure 6.6: Charge-discharge capacity for $LiMn_{2-x}Dy_xO_4$ (x = 0, 0.01, 0.02, 0.03, and 0.04) (a) at C/10 rate, (b) at C/5 rate

The galvanostatsic charge-discharge study at C/5 rate is performed continuously after 10 cycles at C/10 rate to understand the cyclic behavior at elevated C-rate. The initial specific charge and discharge capacities are 64.4, 42.2, 77.5, 57.4, 58.2, and 57.4 $mAhg^{-1}$ and 59.6, 40.3, 72.8, 53.0, 54.8, 56.4 $mAhg^{-1}$ for LMO and $LiMn_{2-x}Dy_xO_4$ (x= 0.01, 0.02, 0.03, 0.04, 0.05) cathode materials, respectively. The columbic efficiency in the initial cycle is 92.54%, 95.49%, 93.93%, 92.43%, 94.18, 98.25% for LMO and $LiMn_{2-x}Dy_xO_4$ (x= 0.01, 0.02, 0.03, 0.04, 0.05) cathodes. The specific discharge capacity after 10 cycles is obtained as 54.1, 37.9, 67.2, 50.8, 49.8, 52.2 $mAhg^{-1}$ for LMO and $LiMn_{2-x}Dy_xO_4$ (x= 0.01, 0.02, 0.03, 0.04, 0.05). After 10 cycles, the capacity fading is observed as 8.02%, 5.95%, 7.69%, 4.69%, 9.12%, 5.18% for LMO and $LiMn_{2-x}Dy_xO_4$ (x= 0.01, 0.02, 0.03, 0.04, 0.05), respectively.

Table 6.4: Charge-Discharge Capacity of $LiMn_2O_4$ and $LiMn_{2-x}Dy_xO_4$ (x = 0.01, 0.02, 0.03, 0.04, 0.05) Cathodes at C/10 Rate

Sample Description	*Charging Capacity ($mAhg^{-1}$)*	*Discharging Capacity ($mAhg^{-1}$)*	*Charging Capacity ($mAhg^{-1}$)*	*Discharging Capacity ($mAhg^{-1}$)*	*Discharge Capacity Fading*	*Columbic Efficiency*
	At 1st cycle	At 1st cycle	At 5th cycle	At 5th cycle	After 5th cycle (%)	Ist cycle (%)
LMO	121.7	118.1	80.6	76.4	35.26	97.52
LMO-Dy01	158.8	124.2	80.0	76.2	38.65	78.48
LMO-Dy02	154.0	124.7	89.7	82.6	33.76	80.51
LMO-Dy03	100.7	81.9	69.01	63.80	22.10	81.33
LMO-Dy04	108.1	93.2	74.5	71.9	22.85	86.21
LMO-Dy05	103.4	95.5	77.0	70.7	25.96	92.51

Table 6.5: Charge-Discharge Capacity of $LiMn_2O_4$ and $LiMn_{2-x}Dy_xO_4$ (x = 0.01, 0.02, 0.03, 0.04, 0.05) Cathodes at C/5 Rate

Sample Description	*Charging Capacity ($mAhg^{-1}$)*	*Discharging Capacity ($mAhg^{-1}$)*	*Charging Capacity ($mAhg^{-1}$)*	*Discharging Capacity ($mAhg^{-1}$)*	*Discharge Capacity Fading*	*Columbic Efficiency*
	At 1st cycle	At 1st cycle	At 5th cycle	At 5th cycle	After 5th cycle (%)	Ist cycle (%)
LMO	64.4	59.6	54.7	54.1	8.02	92.54
LMO-Dy01	42.2	40.3	38.1	37.9	5.95	95.49
LMO-Dy02	77.5	72.8	67.5	67.2	7.69	93.93
LMO-Dy03	57.37	53.03	52.3	50.8	4.69	92.43
LMO-Dy04	58.2	54.8	50.3	49.8	9.12	94.18
LMO-Dy05	57.4	56.4	52.8	52.2	5.18	98.25

To assess the structural stability, the C/10 rate recovery charge-discharge performance is performed upto 5 cycles. The charge-discharge capacities in first cycle are achieved as 61.4, 63.1, 74.4, 60.8, 69.7, 61.4 $mAhg^{-1}$ and 67.3, 60.2, 77.1, 58.8, 65.4, 60.4 $mAhg^{-1}$ for LMO and $LiMn_{2-x}Dy_xO_4$ (x= 0.01, 0.02, 0.03, 0.04, 0.05) cathode materials, respectively. The columbic efficiency in terms of percentage is obtained as 109.60%, 95.40%, 103.69%, 96.71%, 93.83%, and 98.37% in first recovery cycle. The LMO and $LiMn_{1.98}Dy_{0.02}O_4$ are showing more than 100% columbic efficiency in the initial recovery cycle. It may attribute to Li-ion site occupancy in matrix during C/5 discharge. This phenomenon is not observed in further cycles of charge-discharge. The degradation in capacity after 5th cycles are observed as 3.26%, 16.61%, 6.48%, 3.40%, 5.35%, 1.15% at C/10 rate.

Table 6.6: Charge-Discharge Capacity of $LiMn_2O_4$ and $LiMn_{2-x}Dy_xO_4$ (x = 0.01, 0.02, 0.03, 0.04, 0.05) Cathodes at C/10 (Recv.)Rate

Sample Description	*Charging Capacity ($mAhg^{-1}$)*	*Discharging Capacity ($mAhg^{-1}$)*	*Charging Capacity ($mAhg^{-1}$)*	*Discharging Capacity ($mAhg^{-1}$)*	*Discharge Capacity Fading*	*Columbic Efficiency*
	At 1st cycle	At 1st cycle	At 5th cycle	At 5th cycle	After 5th cycle (%)	Ist cycle (%)
LMO	61.4	67.3	66.6	65.1	3.26	109.60
LMO-Dy01	63.1	60.2	53.2	50.2	16.61	95.40
LMO-Dy02	74.4	77.1	74.9	72.1	6.48	103.69
LMO-Dy03	60.8	58.8	60.0	56.8	3.40	96.71
LMO-Dy04	69.7	65.4	64.4	61.9	5.35	93.83
LMO-Dy05	61.4	60.4	61.7	59.7	1.15	98.37

6.3.3 Rate Performance and Its Analysis

The rate performance during charging and discharging cycles at three different rates C10, C5 and C/10 (recv.) upto 5th cycles are presented in Figure 6.8. The rate performance up-to initial five cycles are shown in Figure 6.8 (a). At C/10 rate, the charging capacity is not stable for all cathode sample and found reduction in each cathode. However, the reduction in charge capacity is found more in the LMO-Dy01 and LMO-Dy02 cathode materials. The specific charging capacity is decreasing gradually in other cathode materials. It may be assigned to formation of solid-electrolyte layer in initial few cycles. The charge capacity at C/5 rate is almost stable and same behavior is found during C/10(recv.) cycles. The LMO-Dy02 cathode material is showing high charge capacity at each C rate i.e. C/10, C/5 and C/10 (recv.).

The rate performance during discharge process is also showing similar behavior, Figure 6.8 (b), as observed in charging process. The rate of decrement in capacity at C/10 is more compared to C/5 and C/10 (recv.). The discharge capacities of $LiMn_{2-x}Dy_xO_4$ cathode materials at C/5 are more stable compared to un-doped LMO cathode material. The capacity retention in $LiMn_{1.98}Dy_{0.02}O_4$ cathode is highest among LMO and the other cathode materials.

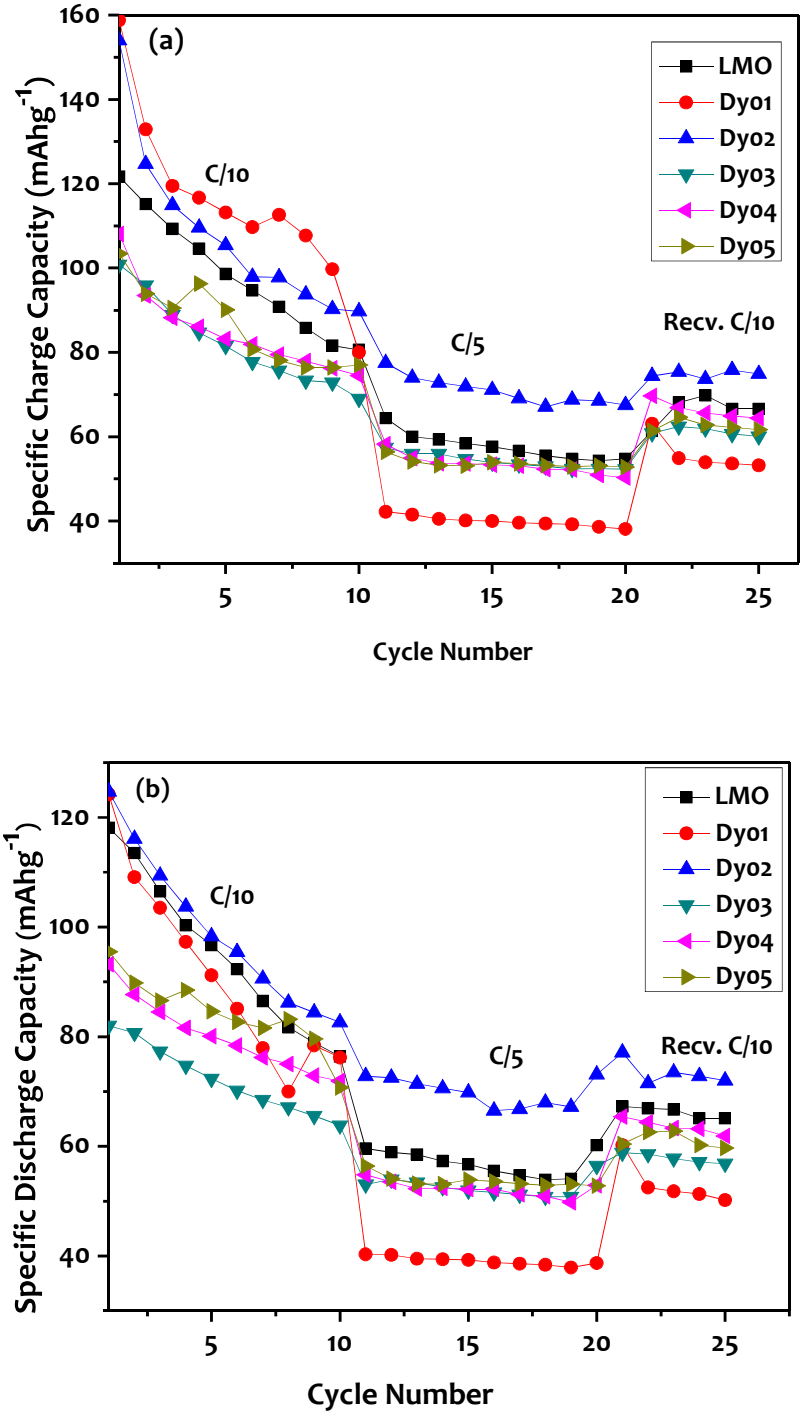

Figure 6.7: Rate performance of $LiMn_2O_4$ and $LiMn_{2-x}Dy_xO_4$ (x = 0.01, 0.02, 0.03, 0.04, 0.05) cathodes in (a) charge process and (b) discharge process at C/10, C/5 and C/10 (recv.)

6.3.3 Electrochemical Impedance Spectroscopy

The electrochemical impedance spectra are recorded by applying 5 mV AC signal over the open circuit voltage and plotted results are shown in Figure 6.8 (a) and enlarge view in inset Figure 6.8 (b). The three electrode Swagelok cell from fabricated LMO and Dy doped cathodes, $LiMn_{2-x}Dy_xO_4$ (x= 0.01, 0.02, 0.03, 0.04, 0.05), are assembled in Ar-atmosphere. The assembling steps of Swagelok cell are covered in sub-section 3.4.1.4 of Chapter 3. The cell internal impedance is found in wide range. The lowest impedance is measured as 170 Ω for the LMO-Dy02 cathode material whereas the highest impedance is observed as 1700 Ω for LMO-Dy01 active material. The internal impedance is observed as 220, 340 and 250 Ω in LMO-Dy03, LMO-Dy04, LMO-Dy05 cathodes, respectively. The un-doped LMO cathode material has large impedance, 2700 Ω, among all the cathode materials. The lowest impedance is observed in Dy doped cathode materials is attributed to reduction in particle size and getting more uniform surface of active material. At low frequency region, the slope is observed almost equal for all the cathode materials. It indicates that diffusion of lithium ion is taking place at same rate during intercalation/de-intercalation process rate. The small radii semi-circle at the mid-frequency region for LMO-Dy02 cathode is showing low charge transfer resistance (R_{ct}). It may assign to thin solid-electrolyte interface layer at the solid and electrolyte interface.

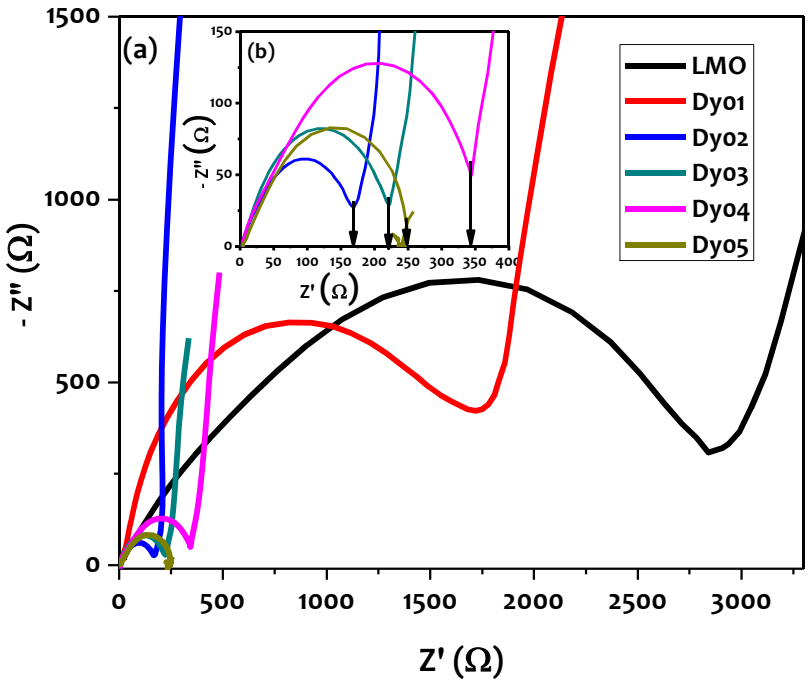

Figure 6.8: EIS spectra of (a) $LiMn_2O_4$ and $LiMn_{2-x}Dy_xO_4$ (x= 0.01, 0.02, 0.03, 0.04, 0.05) cathodes (b) its microscopic view

6.4 CLOSING REMARKS

The rare earth dysprosium elemental doped $LiMn_2O_4$ cathode derivatives, $LiMn_{2-x}Dy_xO_4$ (x= 0.01, 0.02, 0.03, 0.04, 0.05), are synthesized successfully by adopting the organic sol-gel route. The effect of doping amount on physical properties and electrochemical performance is assessed. The Dy elemental doping didn't affect the spinel phase formation. The increased thermal stability and reduced particle size are observed.

The cyclic voltammetry is showing two stage Li^+-ion intercalation and de-intercalation process in all cathodes. The initial charge - discharge capacity for the LMO-Dy02 cathode is 154.0, 77.2, 74.4 and 124.7, 72.8, 77.8 $mAhg^{-1}$ at C/10, C/5 and C10 (recv.) rates. The capacity retention is also observed higher in the LMO-Dy02 spinel cathode.

It is conclusive from above study that the cathode LMO-Dy02 is delivering the higher charge-discharge capacities, improved rate performance at different C-rates, lower charge transfer resistance and low ohmic resistance at higher frequency.